



Contents lists available at ScienceDirect

Journal of Quantitative Spectroscopy & Radiative Transfer

journal homepage: www.elsevier.com/locate/jqsrt

Improving the numerical stability of T-matrix light scattering calculations for extreme particle shapes using the nullfield method with discrete sources

Jens Hellmers^{a,*}, Vladimir Schmidt^a, Thomas Wriedt^b^a Universität Bremen, Badgasteiner Str. 3, 28359 Bremen, Germany^b Institut für Werkstofftechnik, Badgasteiner Str. 3, 28359 Bremen, Germany

ARTICLE INFO

Available online 15 February 2011

Keywords:

T-matrix
Nullfield method
Numerical stability

ABSTRACT

Over the years the T-matrix method based on the nullfield method established itself as a fast and reliable approach for light scattering simulation. Compared to other programs based on discrete dipole approximation or finite difference time domain, programs calculating the T-matrix usually are faster. Unlike the Mie theory the underlying nullfield method can also be used for non-spherical particles, but one will observe a limited numerical stability in this case. Using an advanced approach, the nullfield method with discrete sources, we would like to demonstrate how to improve the numerical stability and to get results also for particles with extreme shapes like fibers or discs with high aspect ratios or concavities. In this paper we intentionally keep the mathematical part rather small, instead we focus on more general explanations for users of corresponding computer programs by outlining basic ideas and concepts.

© 2011 Elsevier Ltd. All rights reserved.

1. Introduction

Waterman's nullfield method (NFM) [1], which is usually used to calculate the T-matrix, can be applied reasonably to nearly spherical particles only. NFM-based computer programs, while popular [2–5], show an increasingly unstable numerical behavior for: (a) particle geometries deviating from spherical shape, (b) particles with large size parameters, (c) particles with high real or imaginary parts of the refractive index. The reasons for this lack of stability are due to the implementation of the mathematical nullfield scheme into numerical algorithms for computer programs, as we will demonstrate in this paper.

On the other side, programs based on the NFM, e.g. by Waterman [1], Barber and Hill [6] or Mishchenko et al. [7,8] usually need significant less computational time compared to programs based on a volume integral

approach like discrete dipole approximation (DDA) [9] or an initial value problem like finite difference time domain (FDTD) [10]. Because of this, using a T-matrix program can be favorable in theoretical light scattering investigations.

To overcome the numerical problems, e.g. Iskander et al. developed the iterative extended boundary condition method (iEBCM) [11]. In the frame of the iEBCM the interior volume of the particle is separated into overlapping subregions, in each of which a separate field expansion is assumed. In other approaches Mishchenko and Travis investigated the benefits of improved numerical precision [12], Voshchinnikov et al. combined elements of the T-matrix ansatz with the separation of variables method (SVM) [13] and Kahmert used irreducible matrix presentations for symmetrical particles [14].

In this paper we would like to demonstrate how the numerical stability of light scattering calculations can be increased by applying an advanced NFM using distributed discrete sources (NFM-DS). This approach was introduced by Doicu et al. [15]. The NFM-DS enables to handle highly non-spherical particles with large aspect ratios and

* Corresponding author.

E-mail address: hellmers@iwt.uni-bremen.de (J. Hellmers).

concavities (case (a) from above list). Additionally, we show how the calculation time benefits from a T-matrix approach.

2. T-matrix and nullfield method approach

The theory of the T-matrix approach has been outlined many times, therefore here we just present the basic steps necessary for understanding the arguments, concepts and results following in this paper. For a detailed description of the underlying mathematics see, e.g. Mishchenko et al. [16] or Doicu et al. [17].

Assuming an electromagnetic plane wave scattered by a single particle, the incident and the scattered fields are expanded into spherical vector wave functions (SVWF) $\mathbf{M}_{mn}(k_s, \mathbf{r})$ and $\mathbf{N}_{mn}(k_s, \mathbf{r})$ (here omitting the time factor $e^{i\omega t}$)

$$\mathbf{E}_{inc}(\mathbf{r}) = \sum_{n=1}^{\infty} \sum_{m=-n}^n a_{mn} \mathbf{M}_{mn}^1(k_s, \mathbf{r}) + b_{mn} \mathbf{N}_{mn}^1(k_s, \mathbf{r}), \quad (1)$$

$$\mathbf{E}_{sca}(\mathbf{r}) = \sum_{n=1}^{\infty} \sum_{m=-n}^n f_{mn} \mathbf{M}_{mn}^3(k_s, \mathbf{r}) + g_{mn} \mathbf{N}_{mn}^3(k_s, \mathbf{r}), \quad (2)$$

$k_s = k_0 \sqrt{\epsilon_s \mu_s}$ is the wave number; a_{mn} , b_{mn} are the expansion coefficients for the incident and f_{mn} , g_{mn} for the scattered field. The index 1 denotes regular and the index 3 radiating solutions of Maxwell's equations in $\mathbb{R}^3 - \{0\}$, see Doicu et al. [17]. These expansion coefficients are related by a linear transformation, the T-matrix:

$$\begin{bmatrix} f_{mn} \\ g_{mn} \end{bmatrix} = \mathbf{T} \begin{bmatrix} a_{mn} \\ b_{mn} \end{bmatrix} = \begin{bmatrix} \mathbf{T}^{11} & \mathbf{T}^{12} \\ \mathbf{T}^{21} & \mathbf{T}^{22} \end{bmatrix} \begin{bmatrix} a_{mn} \\ b_{mn} \end{bmatrix}. \quad (3)$$

The T-matrix contains the whole information about the scattering process except the incident field. This is especially useful for expanded investigations of a scattering problem, e.g. in cases where the incident angle has to be changed or one wants to calculate the orientation averaged scattering diagram. As long as scattering parameters like particle size, shape and refractive index would not change, the T-matrix can be used again. This leads to significant savings of computational time, which will be demonstrated in one of the following sections.

To derive the T-matrix usually the so-called nullfield method (NFM) is used, sometimes called the extended boundary condition method (EBCM) [19]. For this the scatterer is assumed to be a closed domain D_i with a surface S . Using Huygens principle and transmission conditions for the fields at the particle surface one can express the relation between the incident field, the total external field and the surface field on S :

$$\left. \begin{matrix} \mathbf{E}(\mathbf{r}) \\ 0 \end{matrix} \right\} = \mathbf{E}_{inc}(\mathbf{r}) + \text{unknown surface field on } S, \mathbf{r} \begin{cases} \text{outside } D_i \\ \text{inside } D_i. \end{cases} \quad (4)$$

The lower branch of Eq. (4) is also called the nullfield equation:

$$\mathbf{E}_{inc}(\mathbf{r}) + \nabla \times \int_S \mathbf{e}_i(\mathbf{r}') g(k_s, \mathbf{r}, \mathbf{r}') dS(\mathbf{r}') + \frac{j}{k_0 \epsilon_s} \nabla \times \nabla \times \int_S \mathbf{h}_i(\mathbf{r}') g(k_s, \mathbf{r}, \mathbf{r}') dS(\mathbf{r}') = 0, \quad \mathbf{r} \in D_i, \quad (5)$$

\mathbf{E}_i , \mathbf{H}_i are the electric and magnetic amplitudes for the interior field, $\mathbf{e}_i = \mathbf{n} \times \mathbf{E}_i$, $\mathbf{h}_i = \mathbf{n} \times \mathbf{H}_i$, $g(k, \mathbf{r}, \mathbf{r}') = \exp(jk|\mathbf{r} - \mathbf{r}'|) / 4\pi|\mathbf{r} - \mathbf{r}'|$, ($\mathbf{r} \neq \mathbf{r}'$) is the scalar Green's function.

In the frame of the NFM the scattering problem by a single particle is solved as follows:

1. Determine the unknown surface fields \mathbf{e}_i , \mathbf{h}_i as a solution of the surface integral equation (5) for a given incident field $\mathbf{E}_{inc}(\mathbf{r})$.
2. Calculate the wanted scattered field $\mathbf{E}_{sca}(\mathbf{r})$ by inserting the surface fields \mathbf{e}_i , \mathbf{h}_i into the upper branch.

In order to calculate the T-matrix the incident and scattered fields are expressed in terms of localized SVWF and the surface fields are approximated using a complete, linear independent basis of vector functions. In this case, the two surface integral equations mentioned above are transformed to infinite linear systems. Here, we would like to omit explaining the corresponding mathematical procedures as they have been published in detail many times, for example by Mishchenko et al. [18], Kahnert [19] or Doicu et al. [17]. Instead we want to focus on a general description and the resulting constraints that have an effect on the work presented in this paper. In principle, there are three steps to derive the T-matrix in the frame of NFM:

1. reduction of the field expansions to the given number of basis functions,
2. calculation of the surface integrals for the truncated linear systems (incident \leftrightarrow interior, interior \leftrightarrow scattered),
3. calculation of the T-matrix through matrix inversion.

While widely known numerical implementations can be used to transfer this scheme into computer algorithms, there are inevitable limitations. Firstly, 'smooth' integrals in step 2 must be 'reduced' to 'discrete' series expansions. Secondly, the series expansions cannot be done indefinitely—instead there must be a truncation after a sufficient depth.

The question of course is, when the depth of series expansion, which from now on we would like to refer as $Nrank$, is sufficient enough. The realization within a computer program usually is done as follows: a result is calculated for a certain expansion depth $Nrank=i$. Then the depth is increased to $Nrank=j$, a result is calculated again and compared with that from $Nrank=i$. For a simply shaped scatterer one will observe, that the results for an increasing expansion depth $Nrank$ will get closer and closer. So, if the result for $Nrank=j$ does not significantly differ from that for $Nrank=i$ one can assume that the last calculated result is correct and the sought-after one. Usually, the user of a program can define the corresponding threshold; if the change of the results (calculated during the simulation for increasing values of $Nrank$) stays under this limit, the calculation process is stopped. In this case the results show *convergence*.

This convergence should not be mistaken for *numerical unstable* calculations. Here, the results for increasing

expansions depths N_{rank} start to behave unpredictably, usually never reaching convergence. Therefore numerical stable calculations are required so that one can get a converging result.

The different effects ‘convergence’ and ‘numerical unstable calculations’ are drafted in Fig. 1.

The unstable behavior usually is a result of the procedure necessary in step 3, as for example Mishchenko et al. explain [18]. The inversion of a matrix in general is not a trivial numerical process and can be significantly influenced by round off errors. Here, the matrix elements are surface integrals including Hankel and Bessel functions; the Hankel functions of low order have high values while the Bessel functions of high order tend to oscillate. So one has to cope with highly oscillating functions of radius r . By increasing: the particle size and/or the difference between r_{min} and r_{max} (for non-spherical particles) and/or investigating even more complex particle shapes, the matrix element calculation scheme becomes unstable. In other words: there is a direct connection to the particle’s size and more importantly to its shape. The more it differs from a spherical form, the more numerically difficult it gets to calculate the matrix elements. The following inversion process increases these errors and in the end the calculation becomes numerically unstable.

A typical observation is that a behavior (meaning: the very pattern), as presented in Fig. 1 (right), can be reproduced only on the same computer. Running the same program on a different hardware can lead to a different behavior/diagram pattern (while still unstable): Let us assume, that running a NFM program on computer ‘A’ will lead to ‘ r_{A_i} ’ as result for $N_{rank}=i$. Doing the same calculation again on ‘A’ will give the same ‘ r_{A_i} ’. Running

the same program now on a computer ‘B’ might lead to a different result ‘ r_{B_i} ’.

As numerical stability is crucial for light scattering calculations and as it decreases for particle shapes getting more and more complex we would now like to demonstrate how to improve it.

3. Improving the numerical stability

3.1. Using an advanced NFM with discrete sources

A first approach to improve the numerical stability is to replace the localized SVWFs that are used to describe the interior field by using distributed discrete sources. For a comprehensive description of the use of discrete sources in the frame of scattering theory we recommend the books by Doicu et al. [17,15].

In principle, the conventional NFM theory is expanded by using distributed SVWF to describe the interior field

$$\mathcal{M}_{mn}^{1,3}(k\mathbf{r}) = \mathbf{M}_{m,|m|+l}^{1,3}[k(\mathbf{r}-z_n\mathbf{e}_z)],$$

$$\mathcal{N}_{mn}^{1,3}(k\mathbf{r}) = \mathbf{N}_{m,|m|+l}^{1,3}[k(\mathbf{r}-z_n\mathbf{e}_z)], \tag{6}$$

\mathbf{e}_z is the unit vector in z -direction, $n = 1, 2, \dots, m \in \mathbb{Z}$, $l = 1$ for $m=0$, $l=0$ for $m \neq 0$. See also Fig. 2. $\{z_n\}_{n=1}^\infty$ is a set of origins within the inner domain D_i of the scatterer with surface S . For elongated scatterers the sources are placed on the z -axis, for oblate particles the sources are placed in the complex plane $z_n = i\hat{z}_n, \hat{z}_n \in \mathbb{R}$.

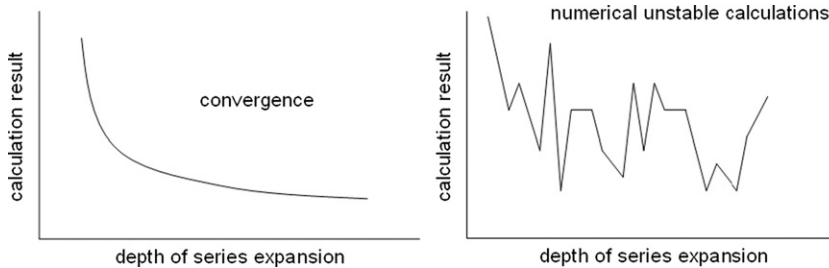


Fig. 1. Sketch to demonstrate the different effects ‘convergence’ and ‘numerical stability’. While on the left hand side the results start to converge to a certain value with an increasing expansion depth, on the right hand side they unpredictably bounce and therefore represent a numerical unstable calculation.

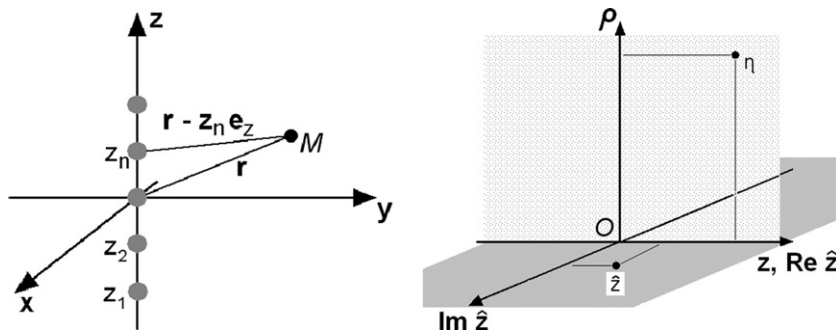


Fig. 2. Concept of discrete sources. Left: along the z -axis. Right: in a complex plane.

Then the conventional nullfield equation (5) is reformulated

$$\nabla \times \int_S [\mathbf{e}_i(\mathbf{r}') - \mathbf{e}_e(\mathbf{r}')] g(k_s, \mathbf{r}, \mathbf{r}') dS(\mathbf{r}') + \frac{j}{k_0 \epsilon_s} \nabla \times \nabla \times \int_S [\mathbf{h}_i(\mathbf{r}') - \mathbf{h}_e(\mathbf{r}')] g(k_s, \mathbf{r}, \mathbf{r}') dS(\mathbf{r}') = 0, \quad \mathbf{r} \in D_i, \quad (7)$$

\mathbf{e}_i , \mathbf{e}_e , \mathbf{h}_i , \mathbf{h}_e are the tangential components of the electric and magnetic fields inside and outside the scatterer. The usage of distributed SVWFs leads to a set of new nullfield equations

$$\frac{jk_s^2}{\pi} \int_S [\mathbf{e}_i(\mathbf{r}') - \mathbf{e}_e(\mathbf{r}')] \cdot \begin{pmatrix} \mathcal{N}_{mn}^{1,3}(k_s \mathbf{r}') \\ \mathcal{M}_{mn}^{1,3}(k_s \mathbf{r}') \end{pmatrix} + j \sqrt{\frac{\mu_s}{\epsilon_s}} [\mathbf{h}_i(\mathbf{r}') - \mathbf{h}_e(\mathbf{r}')] \cdot \begin{pmatrix} \mathcal{M}_{mn}^{1,3}(k_s \mathbf{r}') \\ \mathcal{N}_{mn}^{1,3}(k_s \mathbf{r}') \end{pmatrix} dS(\mathbf{r}') = 0. \quad (8)$$

The next steps are equivalent to those within the frame of the conventional NFM. For details, here we would like to refer again to the book by Doicu et al. [17].

The idea behind the usage of discrete sources is sketched in Fig. 3. In the standard NFM scheme the light scattering process is described by using an expansion into spherical vector wave functions for the incident and the scattered field. This expansion has one origin in the center of the scatterer. As an illustration one can think of the concentric, little waves on the surface of a lake after throwing a stone into the water. As one can see from Fig. 3 (left) these ‘waves’ fit to a circular/spherical shape. The less spherical the shape the less the ‘waves’ fit. If one would throw now several stones in one line, the resulting ‘waves’ would interfere—and by this it is possible to fit also elongated shapes, see Fig. 3 (right). That is—figuratively spoken—the idea behind the NFM-DS.

Note: this explanation as well as Fig. 3 is just a sketch of the idea, a mnemonic that is easy to understand and remember. From the real, mathematical point of view the whole process is different and much more complex. In short words: using distributed SVWFs instead of localized SVWFs leads to a better approximation of the surface field for non-spherical shapes. Additionally distributed SVWFs are also more preferable because of the lower order of the SVWFs. This allows to avoid numerical problems with spherical Bessel and Hankel functions of higher order.

To demonstrate now the advantage of the NFM-DS for numerical stability, we calculate the scattering diagram for an oblate spheroid with a high aspect ratio. To make sure, that the result calculated using the NFM-DS is correct, we compare it with the result gained by another computer program based on a different scattering theory. In this case we choose the discrete sources method (DSM) [20], as this method is well proven for different

kinds of non-spherical particles like elongated fibers [21], oblate discs or erythrocyte [22]. The DSM is based on a generalized point matching method (PMM) approach and there is no T-matrix calculated.

This DSM scattering diagram serves as reference for a set of NFM-DS calculations with an increasing number of series expansions $Nrank$. The procedure is as follows: starting with $Nrank=10$ the depth of series expansion is increased by 2 until $Nrank=100$. As a result we get 46 NFM-DS scattering diagrams. Then, for every NFM-DS scattering diagram the deviation of the differential scattering cross section (DSCS) for every scattering angle θ is compared to the DSM reference; the average is calculated using the residual sum of squares (RSSQ) for each polarization:

$$\text{avg. dev. diag.} = \frac{1}{360} \sum_{\theta=0}^{359} [\text{DSCS}_{\text{DSM}}(\theta) - \text{DSCS}_{\text{NFM-DS}}(\theta)]^2. \quad (9)$$

The resulting deviation is plotted as a function of the expansion depth $Nrank$.

The scatterer is an oblate spheroid with a diameter of $d=3 \mu\text{m}$, a thickness of $D=0.2 \mu\text{m}$ and therefore an aspect ratio of 15:1.

Fig. 4 (left) shows that for increasing values of $Nrank$ (and therefore deeper series expansions) the deviation between NFM-DS and DSM results gets less. Starting from $Nrank=20$ it stays at nearly the same level for perpendicular polarization. For parallel polarization the deviation fluctuates, but always stays lower than for perpendicular polarization. To prove the good congruence between both methods Fig. 4 (right) shows the corresponding scattering diagrams for $Nrank=26$. So, two conclusions can be made from Fig. 4: firstly, by using distributed sources for field expansion it is possible to calculate light scattering by a significant non-spherical particle using the T-matrix approach. Secondly, the result of the NFM-DS calculation converges towards the correct result with an increasing depth of series expansion.

3.2. Using increased numerical precision

A well-known approach to increase the numerical stability is the usage of a higher numerical precision, see, e.g. Mishchenko et al. [12,18,23]. To demonstrate this, we firstly increase the spheroid diameter—see Fig. 4—from 3 to 4 μm . The thickness is kept constant, the aspect ratio increases from 15:1 to 20:1. We again use DOUBLE precision [24] for light scattering calculation. Because particle and aspect ratio are larger, a worse numerical behavior has to be expected. This is confirmed by Fig. 5, which shows the same type of diagrams as Fig. 4.

As one can observe, the numerical stability indeed decreases. The average deviation between the different

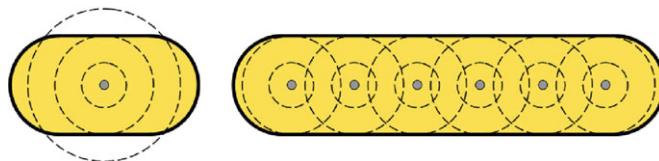


Fig. 3. Sketch to demonstrate the concept behind the NFM-DS.

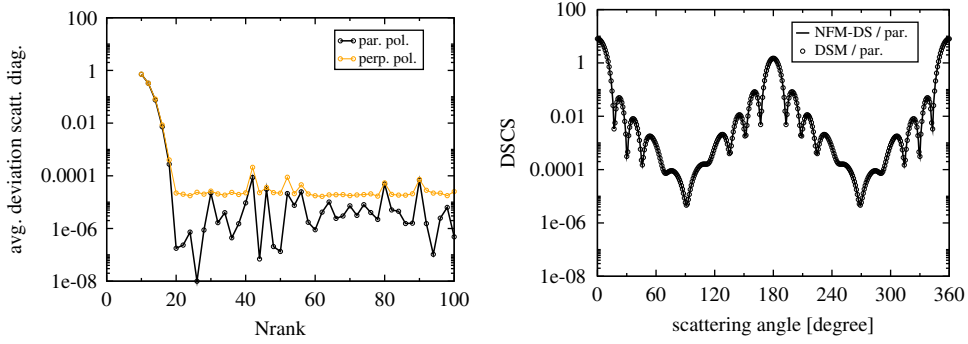


Fig. 4. Influence of the $Nrank$ expansion depth for light scattering calculations using the NFM-DS. The scatterer is an oblate spheroid with a diameter of $d = 3 \mu\text{m}$, a thickness of $D = 0.2 \mu\text{m}$ and therefore an aspect ratio of 15:1. $\lambda = 628.32 \text{ nm}$, refractive index $m = 1.5$, incident angle parallel to rotational axis. Numerical precision is DOUBLE. Left: average deviation between the NFM-DS and DSM scattering diagrams depending on expansion depth $Nrank$. $Nrank$ is increased from 10 to 100, $\Delta Nrank = 2$. Right: Comparison of the NFM-DS and DSM scattering diagram for $Nrank = 26$, parallel polarization.

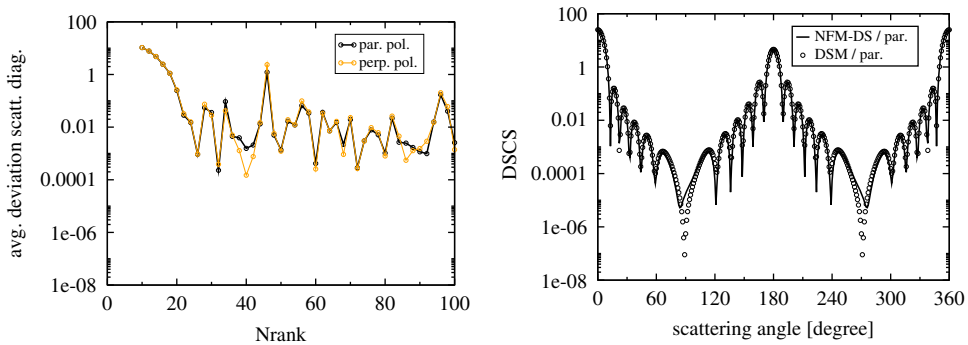


Fig. 5. Lack of convergence for NFM-DS light scattering calculation. The scatterer is an oblate spheroid with a diameter of $d = 4 \mu\text{m}$, a thickness of $D = 0.2 \mu\text{m}$ and therefore an aspect ratio of 20:1. $\lambda = 628.32 \text{ nm}$, refractive index $m = 1.5$, incident angle parallel to rotational axis. Numerical precision is DOUBLE. Left: average deviation between the NFM-DS and DSM scattering diagrams depending on expansion depth $Nrank$. $Nrank$ is increased from 10 to 100, $\Delta Nrank = 2$. Right: Comparison of the NFM-DS and DSM scattering diagram for $Nrank = 32$, parallel polarization.

$Nrank$ expansion depths never converges, Fig. 5 (left) proves that it is a numerically unstable calculation. From all values of $Nrank$ the most promising result could be expected at $Nrank = 32$. The corresponding scattering diagram is presented in Fig. 5 (right). It shows a deviation in side-ward direction.

So, to prove now the benefit from an increased numerical precision, in the next step we change it from DOUBLE to QUAD [24]. This allows to operate with 16 digit floating point numbers during the calculations instead of 8 digit ones. To make the light scattering calculation even more challenging, we again increase the spheroid diameter—here from 4 to 5 μm . Therefore the aspect ratio is 25:1. Fig. 6 presents the diagrams of the light scattering calculation results.

The left graph shows the wanted converging behavior. The average deviation between NFM-DS and DSM results gets smaller and smaller until $Nrank = 30$, after that it increases again, but reaches a steady level from $Nrank = 36$. This general level is higher as observed in Fig. 4, so to check the quality of the results we compare the NFM-DS scattering diagram for $Nrank = 38$ with the DSM reference scattering diagram in Fig. 6. Here, one can observe a very good congruence, the result can be assumed correct.

3.3. Arrangement of discrete sources

The—in general—better numerical stability of the NFM-DS (compared to the conventional NFM) can be improved further by adjusting the position of the discrete sources in a favorable way.

We would like to demonstrate this with an example where we calculate the scattering diagram for a biconcave oblate disc. Concave particle shapes are especially challenging for T-matrix codes, see for example Mishchenko et al. [18]. The most comprehensive investigation of the applicability of a T-Matrix program for concave shapes was done by Wiscombe and Mugnai [25], who used different so-called Chebyshev particles for their studies. However, the investigated particles were—while concave—rather spherical, which made it easier to handle them. Here, we would like to investigate a non-spherical biconcave oblate particle based on a Cassini oval instead. Such a shape can be described using three parameters a , b , and c :

$$y = \pm c \cdot (-a^2 - x^2 \pm (4x^2 a^2 + b^4)^{1/2})^{1/2}. \quad (10)$$

If a is chosen slightly smaller than b , one gets a two-dimensional cross section as presented in Fig. 7. Rotating

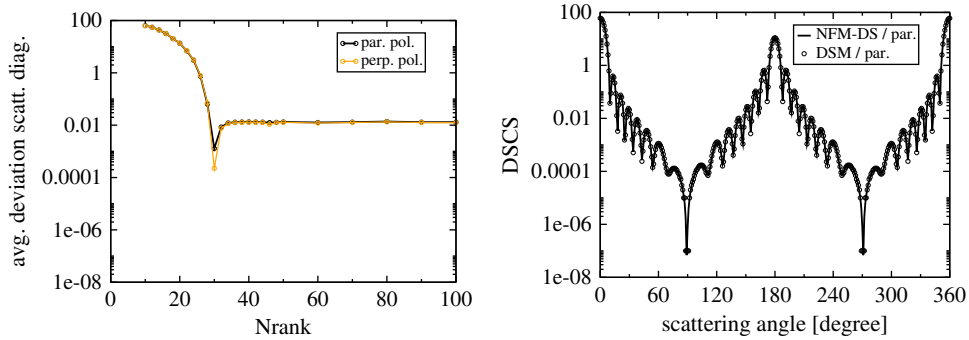


Fig. 6. Converging NFM-DS light scattering results by using higher numerical precision. The scatterer is an oblate spheroid with a diameter of $d = 5 \mu\text{m}$, a thickness of $D = 0.2 \mu\text{m}$ and therefore an aspect ratio of 25:1. $\lambda = 628.32 \text{ nm}$, refractive index $m = 1.5$, incident angle parallel to rotational axis. Numerical precision is QUAD. Left: average deviation between the NFM-DS and DSM scattering diagrams depending on expansion depth $Nrank$. $Nrank$ is increased from 10 to 50 in steps by $\Delta Nrank = 2$ and from 50 to 100 in steps by $\Delta Nrank = 10$. Right: Comparison of the NFM-DS and DSM scattering diagram for $Nrank = 38$, parallel polarization.



Fig. 7. Cross section of the investigated Cassini shape. The Cassini parameters are $a = 1.1 \mu\text{m}$, $b = 1.125 \mu\text{m}$, $c = 0.66$. The resulting diameter is $d = 3.78 \mu\text{m}$ and the aspect ratio is 4:1.

it around its vertical axis gives the three-dimensional particle shape. More details are given in [26].

Fig. 7 shows the particle we would like to discuss here. With these Cassini-parameters and the resulting size and aspect ratio at first it was not possible to get a numerical stable calculation using NFM-DS, even not with QUAD precision. As there is no use of presenting results of numerical unstable calculations the corresponding scattering diagrams are omitted here.

To improve now the numerical behavior we shifted the positions of the discrete sources, which are the origins for the field expansion into SVWFs. Usually, these discrete sources are distributed in the same distance from each other, see Fig. 8 (left). Keeping in mind the sketch from Fig. 3 it seems logical, that in this case such an arrangement might be not favorable for a Cassini oval based shape as in Fig. 7. Therefore we arranged the discrete sources as follows: considering that the Cassini shape is described by polar coordinates $r = r(\theta)$ the section $\theta = -\pi/2, \dots, \pi/2$ is separated into $Nrank + 1$ equal angles θ_{Nrank} . The corresponding values $r = r(\theta_{Nrank})$ are then projected down onto the complex plane, setting a discrete source. As a result for a Cassini oval based shape there is a higher concentration of discrete sources in the middle and the edge of the particle, see also Fig. 8 (right).

By using this distribution of discrete sources we were able to conduct numerical stable calculations. Fig. 9 shows the resulting scattering diagrams for two cases: incident angle of the light parallel to the rotational axis of the scatterer (left) and incident angle between light and rotational axis $\theta = 30^\circ$ (right). To ensure correctness of our results we again compare the diagrams with those gained by DSM. All scattering diagrams show good congruence.

4. Saving computational time

A main advantage of the T-matrix method is that as soon as this matrix is calculated it can be used for additional investigations like changing the direction of the incident light or multiple scattering.

To demonstrate now the time saving advantage of the T-matrix approach we would like to refer to Fig. 9 again. The left diagram shows the scattering diagram for incident light parallel to the rotational axis. For this configuration the T-matrix is calculated. As said, the T-matrix contains all information about the scattering process and is valid, as long as particle size, shape and refractive index is not changed. This T-matrix then is used to calculate the scattering diagram for an angle of 30° between the direction of incident light and the rotational axis of the same scatterer. The corresponding diagram is presented in Fig. 9 (right).

Now, we compare the time necessary to calculate the T-matrix (Fig. 9—left) and the calculation time using the precalculated T-matrix (Fig. 9—right). The calculation times on a PC with an Intel P4 3000 MHz CPU, Intel Fortran compiler, QUAD precision:

- including T-matrix calculation: 24 min,
- using an already calculated T-matrix: 12 s.

As one can see, the necessary calculation time is significantly decreased by using an already calculated T-matrix. This is especially useful in cases where the scattering characteristics for a particle for different directions of incident light has to be calculated. It also allows an easy and fast numerical orientation averaging of a particle's light scattering behavior.

5. Summary and conclusion

In this paper we demonstrate how an advanced T-matrix scheme based on the NFM-DS can be used to calculate light scattering by particles with extreme

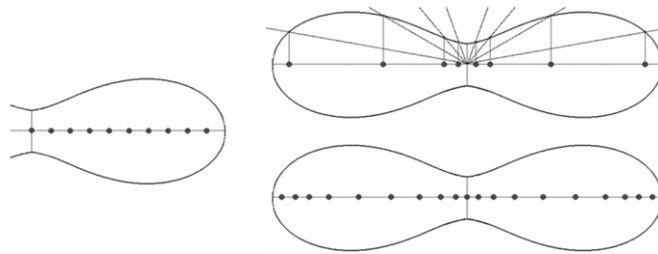


Fig. 8. Left: regular placement, discrete sources distributed in the same distance from each other. Right: improved placement taking into account particle shape.

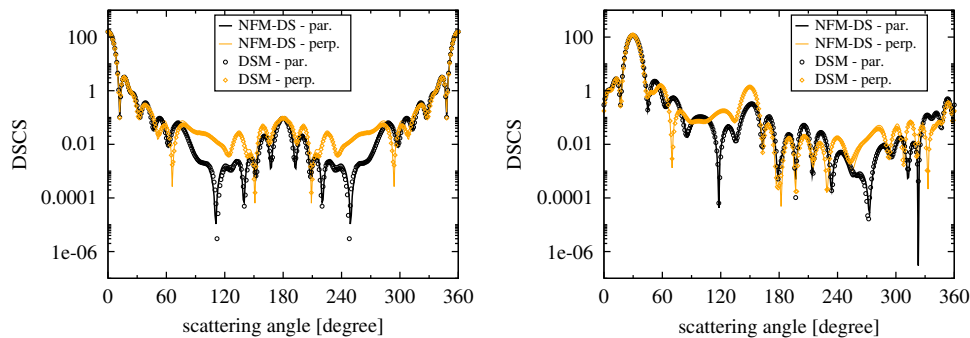


Fig. 9. Scattering diagrams for a biconcave oblate particle based on an oblate Cassini oval as shown in Fig. 7. Wavelength $\lambda = 632.8$ nm, refractive index $m = 1.42$. Left: incident direction is parallel to rotational axis. For this diagram the T-matrix had to be calculated first. On a PC Pentium 4 3000 MHz it took $t = 24$ min (QUAD precision). Right: incident direction is $\theta = 30^\circ$ to rotational axis. For this diagram the already calculated T-matrix could be used. The calculation time in this case was $t = 12$ s (also QUAD precision).

shapes. Our conclusions are as follows:

- The use of distributed discrete sources within the NFM scheme improves the numerical stability in general, as demonstrated by the scattering diagram for an oblate spheroid with a large aspect ratio of 15:1 (Fig. 4).
- Increasing the numerical precision within the light scattering simulation program improves the stability of the calculation even further: while there was no converging result using DOUBLE precision for an oblate spheroid with an aspect ratio of 20:1 (Fig. 5), the scattering pattern of an oblate spheroid with an aspect ratio of 25:1 could be calculated easily using QUAD precision (Fig. 6).
- An aligned distribution of the discrete sources taking into account the particle shape has an additional advantageous influence on the numerical stability of light scattering calculations using the NFM-DS. (Fig. 9).

This enables to use a T-matrix light scattering approach also for highly non-spherical particles with high aspect ratios or even concavities. Usually, for such scatterer programs based on other light scattering theories are used, like discrete dipole approximation (DDA) or finite difference time domain (FDTD). While these programs work reliably, their calculation times usually are longer. The disadvantage regarding the calculation time gets especially significant in cases where light scattering for different directions of the incident light or an orientation averaged scattering

pattern has to be calculated. In such cases the NFM-DS with its feature of using a precalculated T-matrix could be an attractive alternative.

Acknowledgment

We acknowledge the support of this work by Deutsche Forschungsgemeinschaft DFG.

References

- [1] Waterman PC. Matrix formulation of electromagnetic scattering. Proc IEEE 1965;53:805–12.
- [2] Mishchenko MI, Videen G, Babenko VA, Khlebtsov NG, Wriedt T. T-matrix theory of electromagnetic scattering by particles and its applications: a comprehensive reference database. J Quant Spectrosc Radiat Transfer 2004;88(1–3):357–406.
- [3] Mishchenko MI, Videen G, Babenko VA, Khlebtsov NG, Wriedt T. Comprehensive T-matrix reference database: a 2004–06 update. J Quant Spectrosc Radiat Transfer 2007;106(1–3):304–24.
- [4] Mishchenko MI, Videen G, Khlebtsov NG, Wriedt T, Zakharova NT. Comprehensive T-matrix reference database: a 2006–07 update. J Quant Spectrosc Radiat Transfer 2008;109(8):1447–60.
- [5] Mishchenko MI, Zakharova NT, Videen G, Khlebtsov NG, Wriedt T. Comprehensive T-matrix reference database: a 2007–2009 update. J Quant Spectrosc Radiat Transfer 2010;111(4):650–8.
- [6] Barber PW, Hill SC. Light scattering by particles: computational methods. Singapore: World Scientific; 1990.
- [7] Mishchenko M. Light scattering by randomly oriented axially symmetric particles. J Opt Soc Am A 1991;8:871–82.
- [8] Mishchenko M, Travis L. Capabilities and limitations of a current FORTRAN implementation of the T-matrix method for randomly oriented, rotationally symmetric scatterers. J Quant Spectrosc Radiat Transfer 1998;60:309–24.

- [9] Purcell E, Pennypacker C. Scattering and absorption of light by nonspherical dielectric grains. *Astrophys J* 1973;186:705–14.
- [10] Yee S. Numerical solution of initial boundary value problems involving Maxwell's equations in isotropic media. *IEEE Trans Antennas Propag* 1966;14:302–7.
- [11] Iskander M, Lakhtakia A, Durney C. A new procedure for improving the solution stability and extending the frequency range of the EBCM. *IEEE Trans Antennas Propag* 1983;31(2):317–24.
- [12] Mishchenko M, Travis L. T-matrix computations of light scattering by large spheroidal particles. *Opt Commun* 1994;109:16–21.
- [13] Voshchinnikov NV, Il'in VB, Henning T, Michel B, Farafonov VG. Extinction and polarization of radiation by absorbing spheroids: shape/size effects and benchmark results. *J Quant Spectrosc Radiat Transfer* 2000;65:877–93.
- [14] Kahnert M. Irreducible representations of finite groups in the T-matrix formulation of the electromagnetic scattering problem. *J Opt Soc Am A* 2005;22:1187–99.
- [15] Doicu A, Eremin Y, Wriedt T. Acoustic and electromagnetic scattering analysis using discrete sources. Academic Press; 2000.
- [16] Mishchenko M, Hovenier J, Travis L. Light scattering by nonspherical particles. Theory, measurement and applications. Academic Press; 2000.
- [17] Doicu A, Wriedt T, Eremin Y. Light scattering by systems of particles. Springer; 2006.
- [18] Mishchenko MI, Travis LD, Lasis AA. Scattering, absorption and emission of light by small particles. Cambridge: Cambridge University Press; 2002.
- [19] Kahnert F. Numerical methods in electromagnetic scattering theory. *J Quant Spectrosc Radiat Transfer* 2003;79–80:775–824.
- [20] Eremin Y. The method of discrete sources in electromagnetic scattering by axially symmetric structures. *J Commun Tech Electron* 2000;45:269–80.
- [21] Eremina E, Eremin Y, Wriedt T. Review of light scattering by fiber particles with a high aspect ratio. *Recent Res Dev Opt* 2003;3: 297–318.
- [22] Eremina E, Hellmers J, Eremin Y, Wriedt T. Different shape models for erythrocyte: light scattering analysis based on the discrete sources METHOD. *J Quant Spectrosc Radiat Transfer* 2006;102: 3–10.
- [23] Mishchenko M, Travis L, Mackowski D. T-matrix computations of light scattering by nonspherical particles: a review. *J Quant Spectrosc Radiat Transfer* 1996;55:535–75.
- [24] IEEE 754: Standard for binary floating-point arithmetic.
- [25] Wiscombe W, Mugnai A. Single scattering from nonspherical Chebyshev particles: a compendium of calculations. NASA Reference Publication 1985; 1157.
- [26] Hellmers J, Eremina E, Wriedt T. Simulation of light scattering by biconcave Cassini ovals using the nullfield method with discrete sources. *J Opt A* 2006;8:1–9.